electronics

MDPI

Article

A Wideband Metal-Only Patch Antenna for CubeSat

Suhila Abulgasem [1], Faisel Tubbal [1,2,*], Raad Raad [1], Panagiotis Ioannis Theoharis [1], Sining Liu [1] and Muhammad Usman Ali Khan [1]

[1] School of Electrical, Computer and Telecommunications Engineering, University of Wollongong, Wollongong, NSW 2522, Australia; sgsa450@uowmail.edu.au (S.A.); raad@uow.edu.au (R.R.); pit289@uowmail.edu.au (P.I.T.); sl527@uowmail.edu.au (S.L.); muak803@uowmail.edu.au (M.U.A.K.)

[2] Technological Projects Department, The Libyan Center for Remote Sensing and Space Science, Tripoli 21218, Libya

* Correspondence: faisel@uow.edu.au; Tel.: +61-2-4221-8127

Abstract: This article presents a compact wideband high gain patch antenna for CubeSat. The proposed metal-only antenna mainly consists of an upper patch, a folded ramp-shaped patch and shoring pins connecting the antenna with the ground plane. By adjusting the lengths and widths of two arms of the upper F-shaped patch, a second resonant frequency is generated, and hence, the −10 dB bandwidth is increased. Moreover, the effect of arms' lengths and widths on reflection coefficients, operating frequency and bandwidth is presented. To validate the design and the simulation results, a prototype metal-only patch antenna was fabricated and tested in a Chamber. A good agreement between the simulated and measured results is achieved. The measured results show that the fabricated prototype achieves a −10 dB bandwidth of 44.9% (1.6–2.7 GHz), a small reflection coefficient of −24.4 dB and a high efficiency, i.e., 85% at 2.45 GHz. The radiation performance of the proposed antenna is measured, showing a peak realized gain of 8.5 dBi with cross polarization level less than −20 dB at 2.45 GHz and a 3 dB gain bandwidth of 61.22%.

Keywords: CubeSat; antenna; patch antenna; reflection coefficient; gain; bandwidth; polarization

Citation: Abulgasem, S.; Tubbal, F.; Raad, R.; Theoharis, P.I.; Liu, S.; Ali Khan, M.U. A Wideband Metal-Only Patch Antenna for CubeSat. *Electronics* **2021**, *10*, 50. https://doi.org/10.3390/electronics10010050

Received: 31 October 2020
Accepted: 28 December 2020
Published: 30 December 2020

1. Introduction

Cube Satellites (CubeSats) are a class of tiny satellites that have become popular space programs and have opened the door for universities and small companies to gain experience in space technology using cost-effective missions [1]. CubeSats operate at Low Earth Orbit (LEO) at altitudes of 200 km to 800 km, have a mass ranging from 1.3 kg to 6 kg and total volumes of 10 cm × 10 cm × 10 cm (1 U), 10 cm × 10 cm × 20 cm (2 U) and 10 cm × 10 cm × 30 cm (3 U) [2]. Compared with conventional, medium and mini sized satellites, CubeSats have lower mass, are cheaper and are easier to fabricate.

A critical component of CubeSat' telecommunication subsystem that is responsible for establishing the communication link between CubeSats and ground stations is the antenna. Because of the limited real estate of CubeSats, antenna designs must meet the size restriction of CubeSats while yielding high gains and wide bandwidths [3]. Moreover, designed antennas for CubeSats must have a low profile to occupy a small area on CubeSat's surface, thus maximizing the space dedicated to solar panels. The aforementioned challenges can be addressed using patch antenna designs because they have a low profile and are lightweight and cheap. In addition, they have low radiation loss, easy matching of input impedance and are easily integrated with electronic devices [4]. However, their main limitation is their narrow bandwidth, low gains and low efficiency at S-band, i.e., 2.40 GHz [5–7]. For example, in [8], the authors presented S-band transparent mesh patch antenna for 3 U CubeSat. The proposed antenna has a low profile (28.44 mm × 43.7 mm) and an efficiency of 85.9%. However, its main limitation is its narrow −10 dB bandwidth, i.e., 1.67%, and a low gain, 5.3 dBi. Moreover, the authors of [9] proposed a meshed patch antenna that

operates at 2.45 GHz for small satellites. The proposed antenna is integrated with solar cells and fed by two orthogonal feeding ports to achieve circular polarization. It has a small size of 24.1 mm × 24.8 mm, and hence, provides more space for solar cells. Its main limitations are the narrow bandwidth (2.65%) and low gain (4.8 dBi). Another S-band transparent meshed patch antenna is presented in [10]. To improve the antenna's gain and bandwidth, the authors used three transparent meshed patch configurations on CubeSat's surface, which uses the same feeding line. They reported a high gain, of 7.2 dBi, and bandwidth, of 2.65%. Its main limitation, however, is the large antenna size, i.e., 100 mm × 100 mm. In [11], Ygnacio-Espinoza et al. designed a meshed patch antenna for CubeSat applications. The ground plane is made of metamaterial with Reactive Impedance Surface (RIS). This is important as it enhances the bandwidth. The proposed antenna operates at 2.25 GHz and provides a wide bandwidth of 11.1%. However, it has a large antenna size (100 mm × 100 mm) and provides a low gain, of 4.87 dBi.

To address the bandwidth limitation of patch antennas while maintaining a compact size, several techniques have been proposed, such as introducing slots, with popular shapes being the E- and U-shaped patches [12–15] and using shorting pins or walls [16–18]. In addition, by using thick substrates along with the folded patch feeding technique, the impedance bandwidth of patch antennas can be greatly increased [19]. The authors of [12] proposed an E-shaped patch antenna. They placed 25 mm × 27.7 mm asymmetric patch above the ground plane with air substrate between them. The antenna was fed by a folded shaped probe that has unequal arms. They reported a measured impedance bandwidth of 19.8% with an operating frequency of 2.378 GHz. Another E-shaped antenna implementation on a 140 mm × 210 mm ground plane was reported in [13]. The position, the width and the length of the slots was studied to provide an optimal impedance bandwidth of 30.3% at 2.4 GHz using probe feeding and air as substrate material. A symmetric U-slotted patch on a 45.8 mm × 45.8 mm ground plane was studied in [14]. The U-slotted patch antenna was printed on FR4 substrate and was placed 8 mm above the ground plane. As a result, both air and FR4 dielectric were used as substrate material, achieving an impedance bandwidth of 30% at 2.4 GHz. A circular microstrip patch loaded with shorting pins operating at X-band can be found in [17]. The antenna was printed on an RT duroid 5880 and the authors claimed that by adding two balanced shorting pins, the impedance bandwidth was doubled, reaching 8% at 10.8 GHz without affecting the antenna's radiation performance. Finally, the folded patch feeding technique was used in [19], achieving an impedance bandwidth of 73.8% at 2.5 GHz. The E-shaped patch was placed at 20 mm from the ground plane with a shorting wall used to miniaturize the structure while keeping a broad bandwidth.

In this paper, we propose a wideband F-shaped patch antenna for CubeSats communications with an operating frequency of 2.45 GHz. The main idea is to feed the resonance arms of the upper F-shaped patch by a folded patch. This generates two resonant frequencies, and hence, achieves a wide bandwidth. Moreover, three shorting pins between the edges of the upper patch (F-shaped patch) and the ground plane are used to increase the effective electrical length of the patch and hence reduces its physical size. They are also used to lower the resonant frequency and widen bandwidth. The proposed antenna is a metal-only antenna with air substrate. This is important as it presents higher efficiency and improved radiation performance due to the absence of high lossy dielectric substrates [20]. The proposed antenna provides a linear polarization and can be used for establishing up- and downlinks with the ground station. Other proposed linear polarized antennas for satellite communications can be found in [21–24]. Lastly, the performance of the proposed antenna is compared with some existing proposed patch antennas for CubeSat in terms of size, bandwidth and gain.

2. Antenna Configuration and Simulation Results

2.1. Antenna Structure

We selected the folded patch feeding approach with air substrate for our proposed antenna to broaden its impedance bandwidth [19]. Figure 1 shows the geometry of the proposed metal-only patch antenna for CubeSat communications designed to operate at a dominant resonant frequency of 2.45 GHz. The proposed antenna also incorporates shorting pins and a lower folded patch feed. The antenna is mounted on a square ground plane of 100 mm × 100 mm at a distance h_1, uses the air as a substrate and is fed by a 50 Ω coaxial probe at the position (x, y). The presence of the shorting pins in the antenna structure can be considered as adding a shunt inductance in the radiating structure, which enlarges its electrical size by keeping the same physical size and enhancing its radiation performance [16]. The three shorting pins connect the upper patch with the ground plane in order to adjust the lower operating frequency of 1.6 GHz adjacent to the dominant resonant frequency of 2.45 GHz, hence ensuring coupling between the two resonances and wideband operation [25]. The diameter of the shorting pins that provides the optimal antenna bandwidth is 3.64 mm. Moreover, the folded patch technique is used and fed at h_2, to reduce the coaxial probe length and inductance at the feed section. By doing that, a thicker substrate can be used which leads to an improved overall impedance bandwidth [13]. In addition, the use of metal-only patch antenna with air substrate improves the gain of the proposed antenna and ensures zero dielectric losses. The width of the arm W_1 and length of the slot L_2 have a significant effect on the −10 dB bandwidth and the reflection coefficient of the proposed antenna. Therefore, the parametric study is provided using the High Frequency Simulator Structure (HFSS) to determine their optimal values. Table 1 lists the optimal parameters of the proposed antenna. The effect of the shorting pins on the patch is also investigated through the surface current distribution at different frequencies.

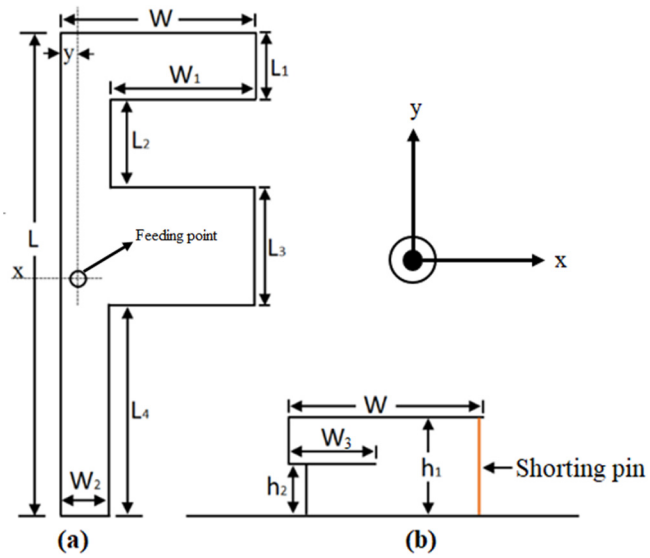

Figure 1. Proposed antenna: (**a**) top view and (**b**) side view.

The F-shaped patch can be considered as a resonant RLC circuit with *R_loss* representing the antenna radiation and losses, as shown in Figure 2a, containing a slot with width W_1 and length L_2. This changes the resonant characteristics of the antenna by introducing an additional current path around the slot [13], which generates an additional lower operating frequency. In other words, this introduces a second RLC resonant circuit with a series inductance *L_low* generated by the slot on the patch as shown in Figure 2b. Therefore, the antenna can be visualized as two RLC resonant circuits, which, when coupled together, can achieve a wider bandwidth.

Table 1. Optimal parameters of the proposed antenna.

Parameters	Values (mm)
W	33.8
L	88.4
W_1	20.8
W_2	10.4
W_3	13
L_1	15.6
L_2	15.6
L_3	20.8
L_4	36.4
h_1	18.4
h_2	9.5
x	0
y	10.4

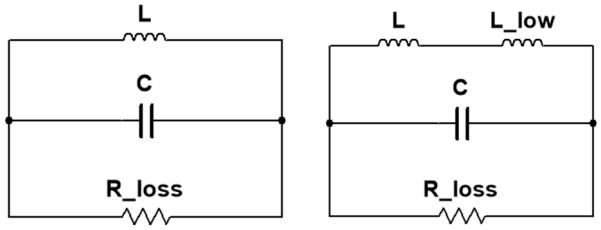

(**a**) (**b**)

Figure 2. Wideband mechanism of the proposed F-shaped patch: (**a**) RLC resonance for 2.45 GHz and (**b**) dual RLC resonance including the effect of the slot.

2.2. Parametric Analysis

This section outlines a parametric study that aims to identify factors that affect antenna performance, i.e., reflection coefficient ($|S_{11}|$), −10 dB bandwidth and total gain. HFSS is used to obtain the simulation results.

The value of W_1 is a vital factor to adjust the resonant frequency of the proposed antenna as it is the main radiating element. Figure 3 shows the simulated $|S_{11}|$ with width W_1 varied from 18.8 to 22.8 mm with 2 mm steps in the range. Other parameters are fixed. We can see that the second (fundamental) resonant frequency shifts downwards (decreases) when increasing width W_1, while the first resonant frequency is barely affected. This is because of the increase of the width of the radiating element. The reason that the lower resonant frequency is barely affected is because it was generated by the shorting pins. Therefore, the width of W_1 has a significant effect on resonant frequency and reflection coefficient of the proposed antenna. To achieve a wide bandwidth and meet the required resonant frequency of 2.45 GHz, W_1 = 22.8 mm is selected. It provides a simulated −10 bandwidth of 1.12 GHz (1.60–2.72 GHz), and small $|S_{11}|$ of −32.8 dB at resonant frequency 2.45 GHz.

Figure 4 shows the simulated $|S_{11}|$ with different slot length values when W_1 = 20.8 mm. The length L_2 is varied from 8.6 to 22.6 mm with 7 mm steps in the range. Other parameters are fixed. We see that the slot length L_2 has no effect on the resonant frequency of the proposed antenna. However, $|S_{11}|$ improves (decreases) when increasing the slot length L_2. In addition, when L_2 is set to 22.6 and 29.6 mm, a dual band resonant mode is obtained instead of only one wide band. The most suitable slot length is L_2 = 15.6 mm as it provides a small $|S_{11}|$ of −32.85 dB at 2.45 GHz and a wide −10 dB bandwidth of 1.12 GHz (1.606 GHz–2.727 GHz). As shown in Figure 5, the width (W_3) of the lower folded patch influences the bandwidth and the operating frequency. We see that when W_3 increases, the operating frequency decreases. For example, when changing W_3 is changed from 7 mm to 16 mm, the operating frequency shifts from 2.62 GHz to 2.37 GHz. Moreover, when W_3 is decreased, e.g., W_3 = 7 mm, the proposed antenna starts providing a dual band instead of a wideband. The optimal width is when W_3 = 15.6 mm, as it provides a

wide −10 dB bandwidth, of 1.08 GHz, with reflection coefficient of −33 dB at the required operating frequency of 2.45 GHz.

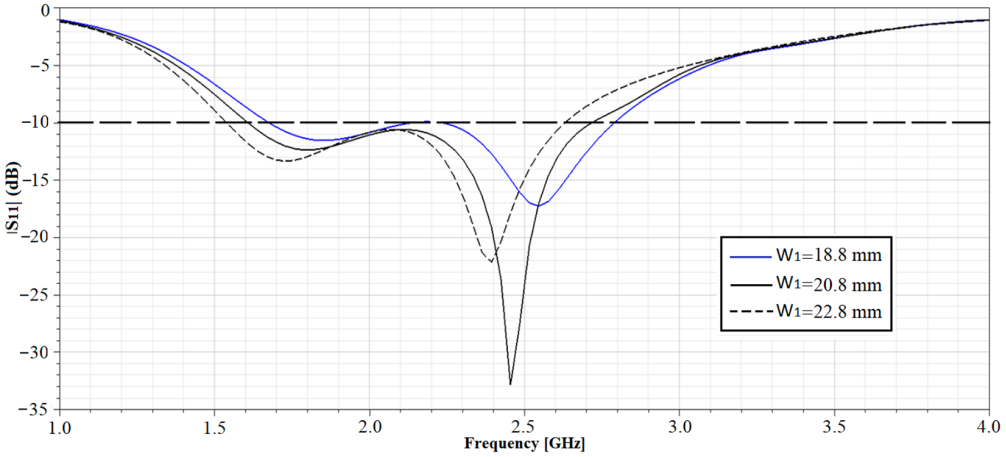

Figure 3. Variation of resonant frequency and reflection coefficient $|S_{11}|$ with respect to width W_1.

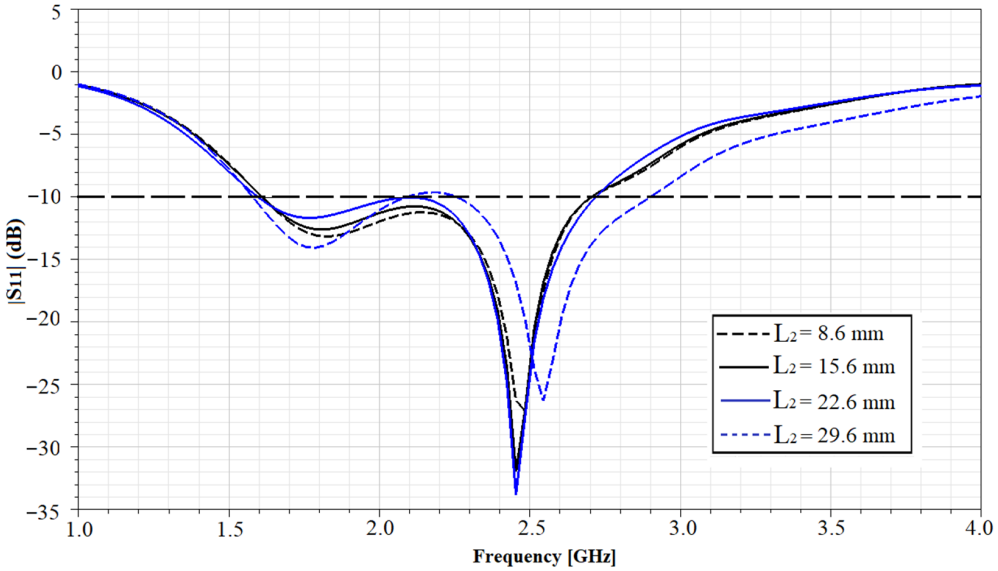

Figure 4. Variation of reflection coefficient $|S_{11}|$ with respect to the length L_2.

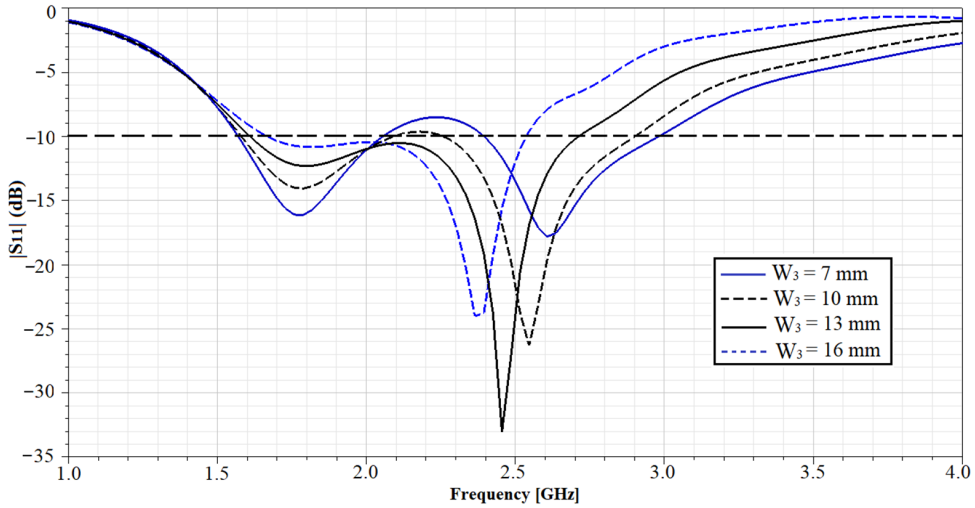

Figure 5. Variation of reflection coefficient $|S_{11}|$ with respect to the length W_3.

Figure 6 depicts the simulated reflection coefficients of the proposed antenna versus a frequency with different values of L_1 (e.g., 10.6 mm, 15.6.8 mm, 20.6 and 30.6 mm). We can see that the change in the L_1 has almost no effect on the −10 dB bandwidth; however, it has a slight effect on the reflection coefficient $|S_{11}|$. We observe that the $|S_{11}|$ increases when the L_1 increases. For example, increasing L_1 from 10.6 mm to 30.6 mm leads to an increase in $|S_{11}|$ from −33.8 dB to −26 dB. The optimal length is when L_1 = 15.6 mm, where it provides a small reflection coefficient of −33.8 dB at 2.45 GHz. As shown in Figure 7, the variation of L_3 has an influence on the reflection coefficient. When L_3 is changed from 20.8 mm (optimal value) to 10.8 mm, the reflection coefficient dramatically increased from −33 dB to −16 dB. This means more power will be reflected back instead of being radiated into space.

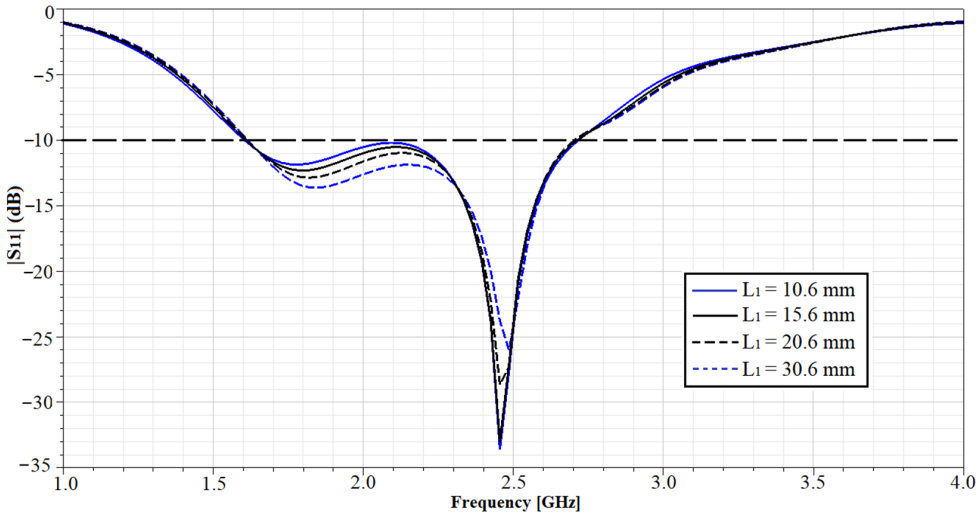

Figure 6. Variation of reflection coefficient $|S_{11}|$ with respect to the length L_1.

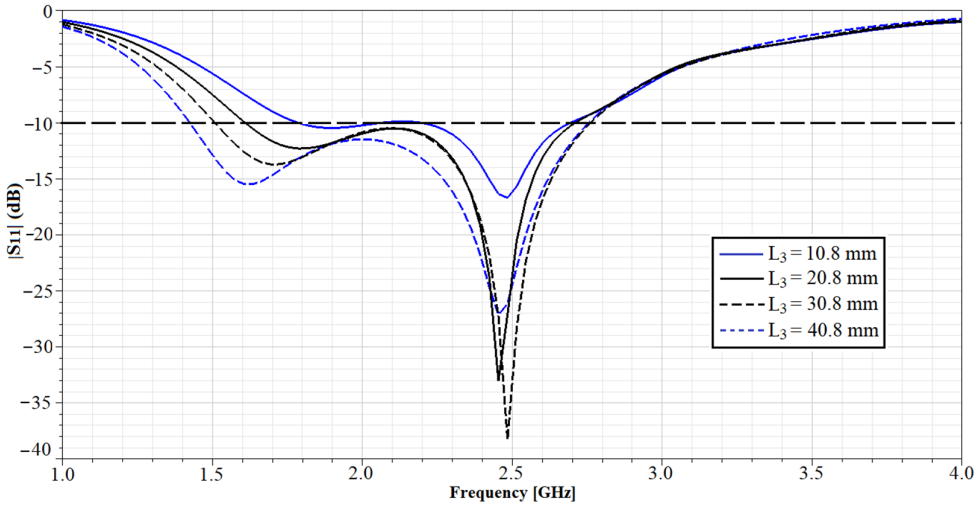

Figure 7. Variation of reflection coefficient $|S_{11}|$ with respect to the length L_3.

2.3. Shorting Pins Investigation

In Figure 8, the effects of shorting pins can be observed based on the surface current distribution on the top radiating F-shaped patch. As can be seen from Figure 8a, the surface current distribution dominates around shorting pin 1 and the top arm of the F-shaped patch as well as shorting pin 2. The current distribution around shorting pin 3 is also more pronounced as compared to the rest of the frequencies (e.g., 1.8 GHz, 2.1 GHz, 2.3 GHz, 2.45 GHz and 2.9 GHz) in Figure 8b–f. This highlights the effect of the three shorting pins on the first resonant frequency of 1.6 GHz. On the other hand, as depicted in Figure 8e,

the surface current is highly concentrated around the middle arm of the F-shaped patch and shorting pin 2, while it weakens around shorting pin 1 and 3. This indicates that the middle arm has a greater effect on the second resonance of 2.45 GHz as compared to the shorting pins.

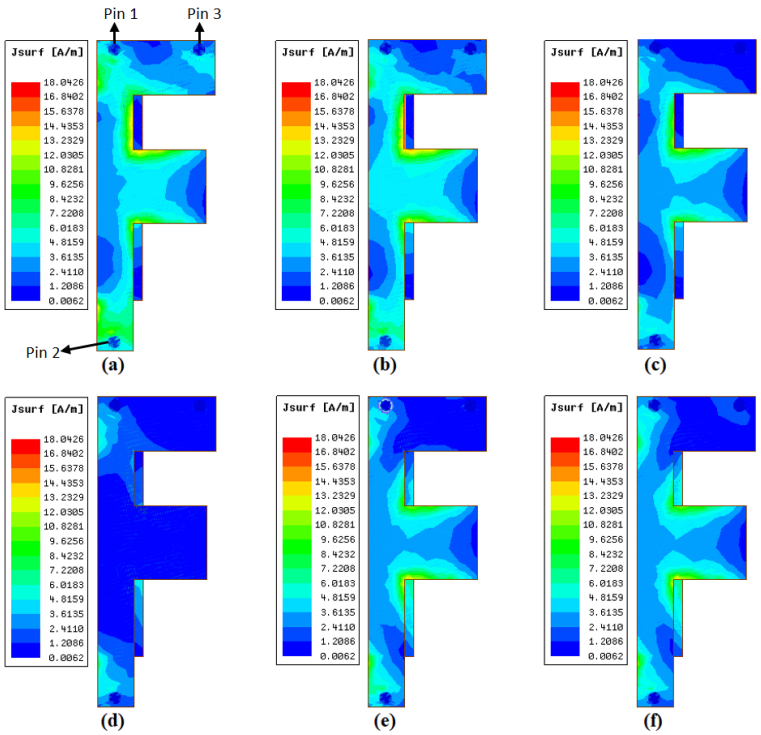

Figure 8. Current distribution on the patch at (**a**) 1.6 GHz, (**b**) 1.8 GHz, (**c**) 2.1 GHz, (**d**) 2.3 GHz, (**e**) 2.45 GHz and (**f**) 2.7 GHz.

Figure 9 shows the simulated $|S_{11}|$ with different diameter values of the shorting pins. The diameter D is varied from 2.64 mm to 5.64 mm, with 1 mm steps in the range. Other parameters are fixed. It can be seen that the pin diameter D has no effect on the resonant frequency and −10 dB bandwidth of the proposed antenna. However, the reflection coefficient $|S_{11}|$ improves (decreases) when D is set to 2.64 mm and 3.64 mm as compared to a diameter of 4.64 mm and 5.64 mm. We can also see that the first resonance is shifted from 2 GHz to 1.8 GHz when D is equal to 4.64 mm and 5.64 mm. The optimal diameter of the shorting pins, which provides a small $|S_{11}|$ at 2.45 GHz and a wideband width, was found to be 3.64 mm. Moreover, the effect of the distance (d_1) between shorting pin 1 and shorting pin 2 and the distance (d_2) between shorting pin 1 and shorting pin 3 on $|S_{11}|$ is shown in Figures 10 and 11, respectively. It is clearly shown that the distance d_1 has a significant effect on the resonant frequency and the matching of the antenna. As the distance d_1 varies from 70.4 mm to 80.4 mm, the proposed antenna achieves a wide –10 dB bandwidth of 1.26 GHz (1.57–2.83 GHz) and a small $|S_{11}|$ of −19 dB at a lower frequency (e.g., 1.7 GHz); however, the operating frequency is shifted to 2.58 GHz. In addition, setting d_1 to 70.4 mm leads to an impedance mismatching across the frequency range 1–3.5 GHz. The optimal distance between pins 1 and 2 is when d_1 = 88.4 mm, as it provides a wide −10 dB bandwidth of 1.08 GHz at the required operating frequency of 2.45 GHz. On the other hand, by varying the distance d_2 from 5.54 mm to 10.54 mm, the operating frequency remains unchanged at 2.45 GHz. The main effect observed when changing d_2 is on the impedance matching, which improves as the shorting pins 1 and 2 are set to 20.54 mm apart. The worst-case impedance matching is observed when d_2 = 5.54 mm, which gives a $|S_{11}|$ of −22 dB. The reflection coefficient is improved by setting d_2 = 20.54 mm to a value of −33 dB.

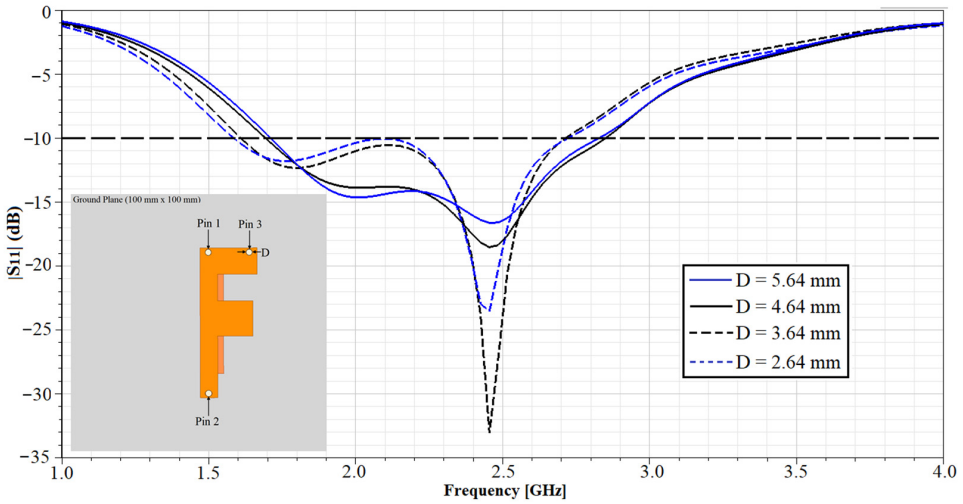

Figure 9. Variation of reflection coefficient $|S_{11}|$ with respect to the diameter (D) of the shorting pins.

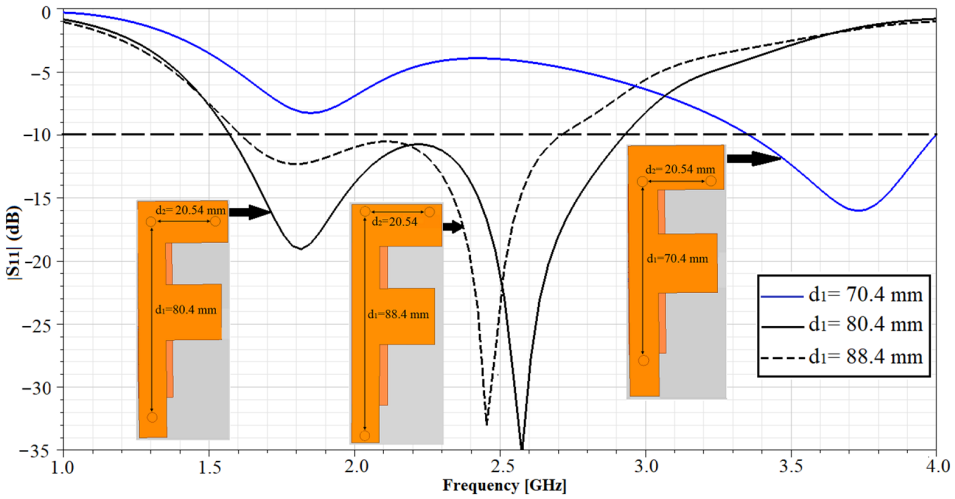

Figure 10. Variation of reflection coefficient $|S_{11}|$ with respect to the shorting pins' positions (d_1).

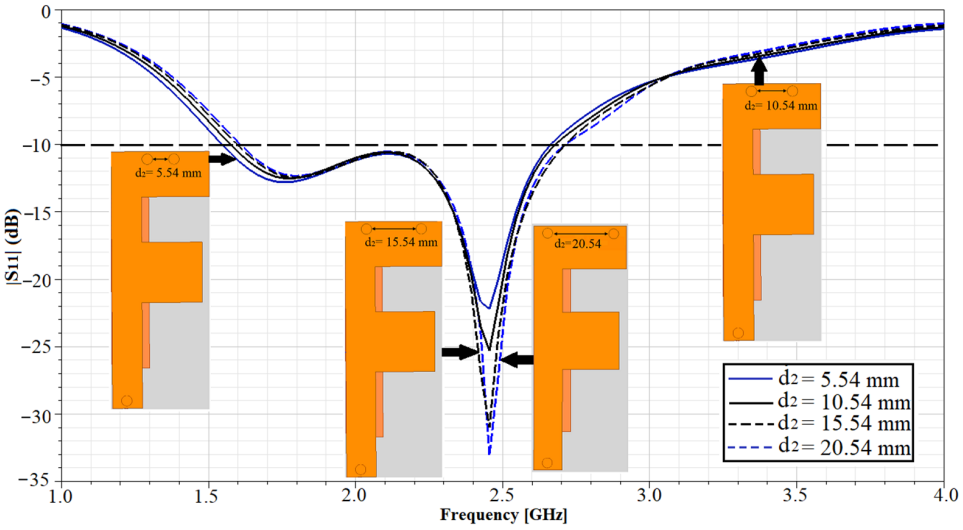

Figure 11. Variation of reflection coefficient $|S_{11}|$ with respect to the shorting pins' positions (d_2).

3. Experimental Results

Antenna Fabrication

The proposed patch antenna is fabricated and measured to verify the simulation results and the approach. As shown in Figure 12, the proposed antenna is fed by a 50 Ω coaxial cable and a feeding pin. For a clear view, the 50 Ω feeding point is enlarged. The proposed antenna is soldered on the ground plane via shorting pins.

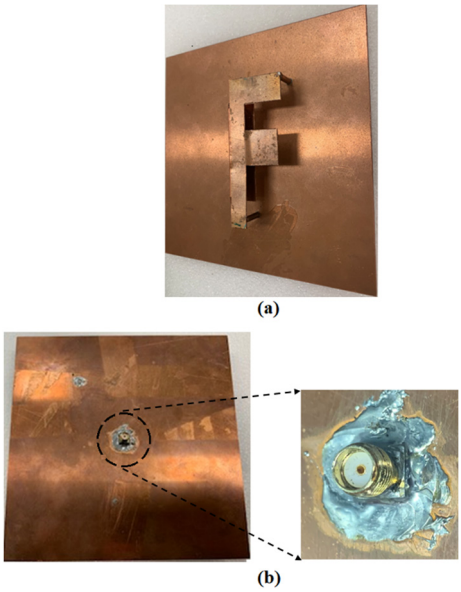

Figure 12. Fabricated prototype of the proposed patch antenna. (**a**) Top view and (**b**) bottom view.

Figure 13 shows the measured and simulated reflection coefficients of the proposed antenna. We see that the measured data generally agree well with the simulated results. The discrepancy between the measured and simulated results at 1.82 GHz is caused by the soldering error and the fabrication inaccuracies. The proposed metal-only patch antenna achieves a measured $|S_{11}| < -10$ dB bandwidth of 1.6–2.7 GHz (44.9%) and a small reflection coefficient of −24.4 dB at 2.45 GHz.

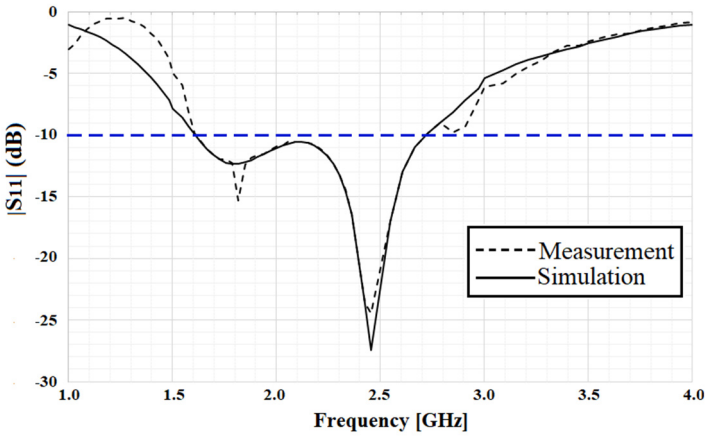

Figure 13. Simulated and measured reflection coefficient of the proposed antenna.

The inset of Figure 14 shows the test setup inside the far-field anechoic chamber located at the University of Wollongong. Our proposed patch antenna is considered as the antenna under test (AUT) and was positioned on a low reflective test turntable. Moreover, the broadband horn antenna was used as a transmitter and the AUT was used as a receiver. The measurements distance between the transmitter and the AUT was set to 3 m to ensure

the AUT lied in the far-field radiation zone during the experiment. We connected the AUT and the horn antenna to port one and port two of the Vector Network Analyzer (VNA), respectively. The test setup was calibrated with a Keysight 85519A 50-Ω calibration kit and a characterized female SMA to male N-connector adapter. We set the VNA to transmit at 2.45 GHz with an output power of 0 dBm. The S_{12} quantity was then observed to obtain the received power on port one ratioed to 0 dBm for the principal E and H planes. Finally, the VNA was interfaced with MATLAB to plot the measured radiation pattern for 2.45 GHz.

Figure 14 depicts the measured and simulated radiation patterns of the proposed antenna in E-plane (x-z-plane) and H-plane (y-z-plane). The measured and simulated results are in good agreement. We see that in x-z-plane, the level of cross-polarization is higher than the cross-polarization in y-z-plane. This is because the use of shorting pins and the feed location generates higher order modes by introducing asymmetry of the antenna's structure and consequently generates the cross-polarized radiation patterns. The proposed antenna achieves a maximum gain of 8.5 dBi with a -30° tilt off broadside in the radiation pattern. This is because the proposed antenna has an asymmetric structure.

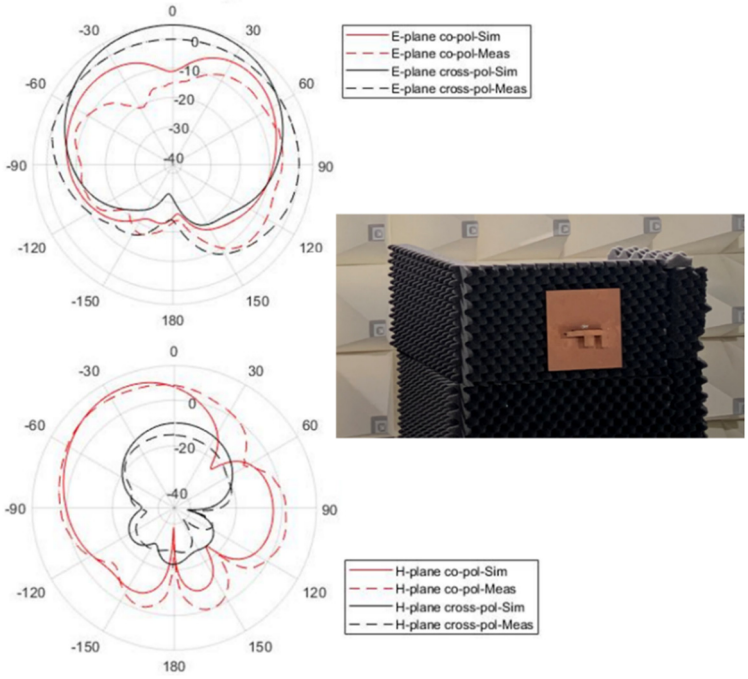

Figure 14. Measured and simulated radiation patterns in (top) x-z-plane (E-plane) and (bottom) y-z-plane (H-plane) at 2.45 GHz (inset: antenna under measurement).

Table 2 presents a detailed comparison between the proposed antenna and published patch antenna designs for CubeSat communications. All bandwidths refer to $|S11| < -10$ dB. It can be clearly observed that the proposed antenna has higher gain, significantly wider bandwidth and adequate dimensions to be integrated with a CubeSat.

Table 2. Comparison of the proposed antenna with previous S-band patch antenna designs.

Ref.	Antenna Size (mm)	Bandwidth $\lvert S_{11} \rvert < -10$ dB (%)	Gain (dBi)
[10]	100 × 100	2.56	7.2
[9]	24.1 × 24.1	1.45	4.8
[26]	110 × 110	9.77	5.4
[27]	100 × 100	35	4
[28]	83 × 83	13	3.5
[29]	80 × 180	11	5.2
This work	100 × 100	44.9	8.5

To evaluate the broadband characteristics of the proposed antenna, the measured and simulated gains versus frequency is presented in Figure 15. The measured 3 dB gain bandwidth of the proposed antenna is 61.22% with a peak gain of 8.5 dBi at 2.45 GHz, indicating that an acceptable gain can be maintained within the operating frequency range. The measured and simulated efficiency of the proposed antenna can be seen in Figure 16, which is highly correlated with ohmic losses in the metallic structure of the antenna as well as impedance mismatching between the folded patch and the probe feed. The efficiency fluctuates between 82% and 88% from 2.2 GHz to 3.7 GHz. Therefore, the proposed patch antenna can achieve a high radiation of 85% at 2.45 GHz, while it can maintain an efficiency higher than 71% from 1.5 GHz to 4 GHz.

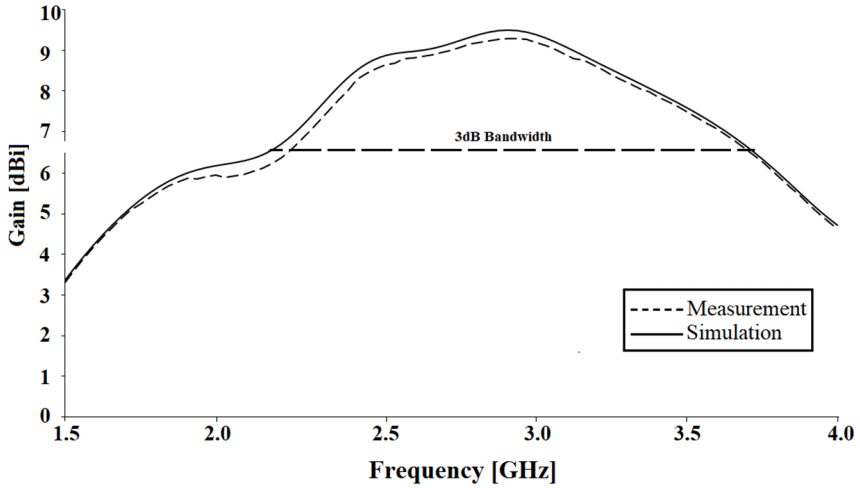

Figure 15. Measured and simulated gains of the proposed antenna.

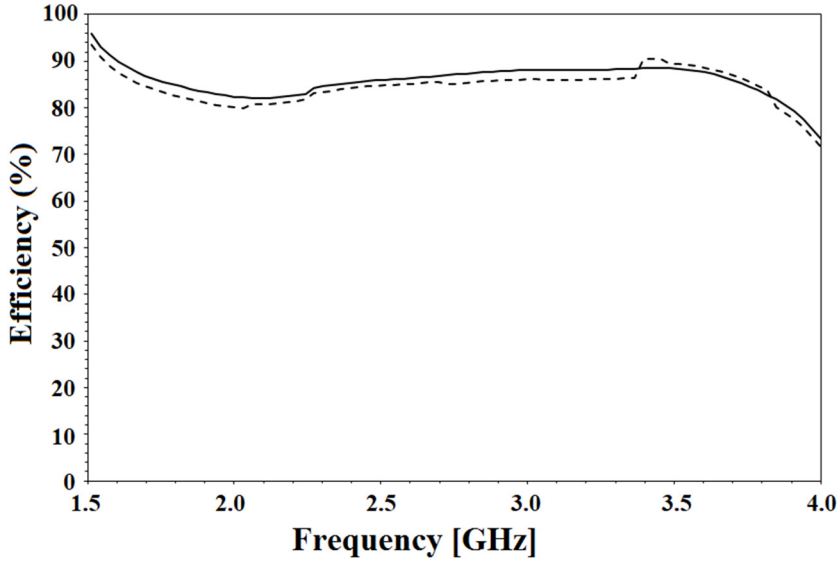

Figure 16. Measured and simulated efficiency of the proposed antenna.

4. Conclusions

A metal-only wideband folded patch antenna for CubeSat applications is demonstrated. A wide bandwidth is achieved by using the folded ramp shaped patch approach to feed the arms of the upper radiating patch. Moreover, to reduce the antenna size, shorting pins are used to connect the upper patch to the ground plane, and hence, increase the patch's effective electrical length and reduce its physical size. To increase the efficiency and improve the performance, the proposed antenna uses air substrate. An antenna re-

alization with an overall size of 100 mm × 100 mm is presented with a bandwidth of 44.9% (1.6–2.7 GHz) for $|S_{11}| < -10$ dB and total gain of 8.5 dBi at 2.45 GHz. Moreover, the proposed antenna provides a high efficiency, of 85%, and a 3 dB gain bandwidth of 61.22%. The measurement results prove the wide bandwidth of the antenna and shows good agreement of the radiation pattern with simulation results.

As a recommendation for future work, to increase the robustness of our proposed antenna for CubeSat applications where the size of the CubeSat platform exceeds the 3 U standard, the air substrate of the proposed antenna could be filled with foam material (dielectric constant) without sacrificing the performance in terms of gain or impedance bandwidth. To finally assess the suitability and durability of our antenna during the CubeSat launch, vibration and shock testing must be performed.

Author Contributions: Design and concept, F.T. and S.A.; methodology, F.T., S.A. and P.I.T.; Investigation, R.R., P.I.T. and S.L.; validation, F.T., S.A., P.I.T. and M.U.A.K.; investigation, F.T. and P.I.T.; resources, F.T., R.R. and P.I.T.; writing—original draft preparation, F.T. and S.A.; writing—review and editing, R.R., P.I.T., S.L. and M.U.A.K.; supervision, R.R. and F.T.; project administration, F.T., R.R., S.A. and P.I.T. All authors have read and agreed to the published version of the manuscript.

Funding: This research received no external funding.

Institutional Review Board Statement: Not applicable.

Informed Consent Statement: Not applicable.

Data Availability Statement: Not applicable.

Conflicts of Interest: The authors declare no conflict of interest.

References

1. Tubbal, F.; Raad, R.; Chin, K.-W.; Matekovits, L.; Butters, B.; Dassano, G. A high gain S-band slot antenna with MSS for CubeSat. *Annals Telecommun.* **2018**, *74*, 223–237. [CrossRef]
2. Tubbal, F.; Raad, R.; Chin, K.-W. A Survey and Study of Planar Antennas for Pico-Satellites. *IEEE Access* **2015**, *3*, 2590–2612. [CrossRef]
3. Woellert, K.; Ehrenfreund, P.; Ricco, A.J.; Hertzfeld, H. Cubesats: Cost-effective science and technology platforms for emerging and developing nations. *Adv. Space Res.* **2011**, *47*, 663–684. [CrossRef]
4. Liu, H.-C.; Horng, T.-S.; Alexopoulos, N. Radiation of printed antennas with a coplanar waveguide feed. *IEEE Trans. Antennas Propag.* **1995**, *43*, 1143–1148. [CrossRef]
5. Liang, J.; Yang, H.-Y.D. Radiation Characteristics of a Microstrip Patch over an Electromagnetic Bandgap Surface. *IEEE Trans. Antennas Propag.* **2007**, *55*, 1691–1697. [CrossRef]
6. Sanchez-Hernandez, D.; Robertson, I.D. A survey of broadband microstrip patch antennas. *Microw. J.* **1996**, *39*, 60–71.
7. Theoharis, P.I.; Raad, R.; Tubbal, F.; Khan, M.U.A.; Liu, S. Software Defined Radios for CubeSat Applications: A Brief Review and Methodology. *IEEE J. Miniat. Air Space Syst.* **2020**, 1. [CrossRef]
8. Neveu, N.; Garcia, M.; Casana, J.; Dettloff, R.; Jackson, D.R.; Chen, J. Transparent microstrip antennas for CubeSat applications. In Proceedings of the IEEE International Conference on Wireless for Space and Extreme Environments, Baltimore, MD, USA, 7–9 November 2013; pp. 1–4.
9. Podilchak, S.K.; Comite, D.; Montgomery, B.K.; Li, Y.; Buendia, V.G.-G.; Antar, Y.M.M. Solar-Panel Integrated Circularly Polarized Meshed Patch for Cubesats and Other Small Satellites. *IEEE Access* **2019**, *7*, 96560–96566. [CrossRef]
10. Yasin, T.; Baktur, R. Bandwidth Enhancement of Meshed Patch Antennas through Proximity Coupling. *IEEE Antennas Wirel. Propag. Lett.* **2017**, *16*, 2501–2504. [CrossRef]
11. Ygnacio-Espinoza, A.; Penaloza-Aponte, D.; Alvarez-Montoya, J.; Mesco-Quispe, A.; Arenas, M.C. Quasi-transparent meshed and circularly polarized patch antenna with metamaterials integrated to a solar cell for S-band CubeSat applications. In Proceedings of the 2018 International Conference on Electromagnetics in Advanced Applications (ICEAA), Cartagena des Indias, Colombia, 10–14 September 2018; pp. 605–608.
12. Xiong, J.; Ying, Z.; He, S. A Broadband Low Profile Patch Antenna of Compact Size with Three Resonances. *IEEE Trans. Antennas Propag.* **2009**, *57*, 1838–1843. [CrossRef]
13. Yang, F.; Zhang, X.-X.; Ye, X.; Rahmat-Samii, Y. Wide-band E-shaped patch antennas for wireless communications. *IEEE Trans. Antennas Propag.* **2001**, *49*, 1094–1100. [CrossRef]
14. Khodae, G.F.; Nourinia, J.; Ghobadi, C. A practical miniaturized u-slot patch antenna with enhanced bandwidth. *Prog. Electromagn. Res. B* **2008**, *3*, 47–62. [CrossRef]
15. Basavarajappa, V.; Vinoy, K.J. An integrated wideband multifunctional antenna using a microstrip patch with two U-slots. *Prog. Electromagn. Res.* **2010**, *22*, 221–235.

16. Zhang, X.; Zhu, L. Gain-Enhanced Patch Antennas with Loading of Shorting Pins. *IEEE Trans. Antennas Propag.* **2016**, *64*, 3310–3318. [CrossRef]
17. Guha, D.; Antar, Y.M.M. Circular Microstrip Patch Loaded With Balanced Shorting Pins for Improved Bandwidth. *IEEE Antennas Wirel. Propag. Lett.* **2006**, *5*, 217–219. [CrossRef]
18. Quevedo-Teruel, O.; Pucci, E.; Rajo-Iglesias, E. Compact Loaded PIFA for Multifrequency Applications. *IEEE Trans. Antennas Propag.* **2009**, *58*, 656–664. [CrossRef]
19. Chiu, C.; Wong, H.; Chan, C. Study of small wideband folded-patch-feed antennas. *IET Microw. Antennas Propag.* **2007**, *1*, 501. [CrossRef]
20. Chahat, N.; Cook, B.; Lim, H.; Dl, P.E. All-Metal Dual-Frequency RHCP High-Gain Antenna for a Potential Europa Lander. *IEEE Trans. Antennas Propag.* **2018**, *66*, 6791–6798. [CrossRef]
21. Vazquez-Alvarez, A.J.; Tubio-Pardavila, R.; Gonzalez-Muino, A.; Agelet, F.A.; Arias-Acuña, M.; Vilan-Vilan, J.A. Design of a Polarization Diversity System for Ground Stations of CubeSat Space Systems. *IEEE Antennas Wirel. Propag. Lett.* **2012**, *11*, 917–920. [CrossRef]
22. Dicandia, F.A.; Genovesi, S. A Compact CubeSat Antenna with Beamsteering Capability and Polarization Agility: Characteristic Modes Theory for Breakthrough Antenna Design. *IEEE Antennas Propag. Mag.* **2020**, *62*, 82–93. [CrossRef]
23. Novak, M.H.; Volakis, J.L. Ultrawideband Antennas for Multiband Satellite Communications at UHF–Ku Frequencies. *IEEE Trans. Antennas Propag.* **2015**, *63*, 1334–1341. [CrossRef]
24. Karabinis, P.D. Satellite Communications Systems and Methods using Diverse Polarizations. Google Patents. U.S. Patent No. 7,636,546, 22 December 2009.
25. Zhong, S.; Lo, Y. Single-element rectangular microstrip antenna for dual-frequency operation. *Electron. Lett.* **1983**, *19*, 298–300. [CrossRef]
26. Yao, Y.; Liao, S.; Wang, J.; Xue, K.; Balfour, E.A.; Luo, Y. A New Patch Antenna Designed for CubeSat: Dual feed, L\/S dual-band stacked, and circularly polarized. *IEEE Antennas Propag. Mag.* **2016**, *58*, 16–21. [CrossRef]
27. Veljovic, M.J.; Skrivervik, A.K. Aperture-Coupled Low-Profile Wideband Patch Antennas for CubeSat. *IEEE Trans. Antennas Propag.* **2019**, *67*, 3439–3444. [CrossRef]
28. Tubbal, F.E.; Raad, R.; Chin, K.-W.; Butters, B. S-band shorted patch antenna for inter pico satellite communications. In Proceedings of the 2014 8th International Conference on Telecommunication Systems Services and Applications (TSSA), Denpasar, Indonesia, 23–24 October 2014; pp. 1–4.
29. Lobato-Morales, H.; Villarreal-Reyes, S.; Guerrero-Arbona, E.; Martinez-Aragon, E.; Chavez-Perez, R.A.; Medina-Monroy, J.L.; Figueroa-Torres, C.A. A 2.45-GHz Circular Polarization Closed-Loop Travelling-Wave Antenna for Cubesats. In Proceedings of the 2019 International Conference on Electronics, Communications and Computers (CONIELECOMP), Cholula, Mexico, 27 February–1 March 2019; pp. 154–157.